# Reactions of Organosulfur Compounds with Si(100)

**Zuoming Zhu,† Abneesh Srivastava, and Richard M. Osgood, Jr.***

*Columbia Radiation Laboratory, Columbia University, New York, New York 10027*

*Received: March 28, 2003; In Final Form: July 31, 2003*

Room-temperature adsorption of three model organosulfur compounds, dimethyl disulfide ($CH_3SSCH_3$), methanethiol ($CH_3SH$), and dimethyl sulfide ($CH_3SCH_3$), on Si(100) has been investigated using Auger electron spectroscopy (AES), low-energy electron diffraction (LEED), temperature-programmed desorption (TPD), and density functional theory (DFT) calculations. AES measurements show that each of these organosulfur compounds has a characteristic surface saturation coverage and reaction probability with Si(100). TPD studies indicate that methyl groups of these organosulfur compounds remain intact upon adsorption on Si(100). DFT calculations, in conjunction with our experimental results, provide insight into the most likely chemisorption channel for each organosulfur compound.

## I. Introduction

Chemical functionalization of the reconstructed surface of silicon has become an important research area. In part, this derives from the desire to marry the chemical flexibility of organic materials with the most important inorganic platform for electronics, namely, single-crystal silicon.[1−4] In particular, the interest in producing high-quality ultrathin films of organic molecules on Si(100) has motivated a widespread interest in understanding the reaction of unsaturated organics with the unpaired electrons of the dimers on this surface. This approach is motivated by using the methods of synthetic chemistry to bond directly functional molecular species to specific surface chemical sites rather than using physical methods, such as spin casting, to obtain the organic layer.

In the initial studies, reactions of alkenes with silicon surfaces were extensively studied using a wide variety of experimental methods, such as scanning tunneling microscopy (STM), x-ray photoelectron spectroscopy (XPS), Fourier transform infrared spectroscopy (FTIR), and near-edge X-ray absorption fine structure (NEXAFS), as well as ab initio calculations. These unsaturated hydrocarbons can covalently bond to Si(100) through the [2 + 2] or [4 + 2] or both cycloaddition reactions of C═C, C≡C, and diene functional groups with Si surface dimers. Generally, this distinctive surface chemistry was found to be closely related to the tendency of the buckled Si dimer to form double bonds, that is, a strong $\sigma$-bond and a weak $\pi$-bond.[5−7] Recently, it has been shown that cycloaddition reactions on the Si(100) are not limited solely to alkenes. For example, Ellison et al. have demonstrated the possibility of a cycloaddition reaction involving the N═N bond.[8] In related studies, the reactivity of this same silicon surface with alcohols[9,10] and amines[11−14] has been examined. In general, those investigations of amines have found that the silicon dimers undergo nucleophilic reactions with N−H groups via N lone-pair attack on the lower silicon atom and hydrogen transfer to the upper dimer atom.

At the same time, research in developing new routes to very-low-temperature epitaxial growth has been pursued. One of these techniques has examined the use of direct surface reactions of sequentially dosed molecular precursors with an ultrahigh-vacuum-prepared semiconductor surface to achieve epitaxial growth.[15−22] In this method, epitaxy is achieved not via thermodynamics, using high temperature to promote surface diffusion into equilibrium lattice positions, but rather by direct reaction into a specific lattice position using the directional properties of surface bonds. In general, the chemical questions for this research direction are very similar to those encountered in surface functionalization. For example, several recent studies have examined the reaction of $H_2S$ with Si(100) with this goal in mind.[23−26] In fact, the $H_2S$ chemisorption system illustrates some of the important factors in silicon-surface reactivity. These studies have used ultrahigh vacuum (UHV) probes such as STM, UV photoelectron spectroscopy (UPS), and temperature-programmed desorption (TPD), as well as ab initio computation. The results have shown that $H_2S$ dissociates into S−H and H at low temperatures, that is, below −125 °C, and low coverage, that is, ≤0.25 ML, after inserting into a dimer bond. In addition, at higher temperature, that is, above −75 °C, evidence has been found for the S−H group dissociating to form a bridge bond between neighboring dimers and with the remaining hydrogen atoms saturating the two dangling bonds of the dimer complex. At high coverage (≥0.25 ML of $H_2S$), the adsorption geometry rearranges in such a way that each S atom inserts into the $\sigma$-bond of the dimer so as to form a bridge bond between the two Si atoms with each Si atom also being hydrogen-terminated. Saturation coverage at room temperature is then found to be 0.5 ML.

The present work is motivated by the latter consideration, that is, to understand reactions of molecular-based precursors for epitaxial growth on silicon. We have studied the reaction of several model organosulfur compounds, dimethyl disulfide ($CH_3SSCH_3$), methanethiol ($CH_3SH$), and dimethyl sulfide ($CH_3SCH_3$), with Si(100) at room temperature. These organosulfur compounds hold promise for use as precursors in the growth of sulfur-containing group II−VI materials on silicon. In addition, our studies have used $H_2S$/Si(100) as an experimental and computational benchmark. Understanding the surface chemistry of these organosulfur precursors on Si(100) is important for exploring the chemical strategies for extending

* Corresponding author. E-mail: osgood@columbia.edu. Fax: (212)-860-6182.

† E-mail: zuoming@cumsl.ctr.columbia.edu.

10.1021/jp034803v CCC: $25.00 
Published on Web 11/19/2003

of our previous successful atomic layer epitaxial methodology[20,21] to chemically controlled low-temperature heteroepitaxial growth of II−VI semiconductors on silicon. Our investigation uses UHV probes including Auger electron spectroscopy (AES), low-energy electron diffraction (LEED), and temperature-programmed desorption (TPD) and calculations using density functional theory (DFT).

This paper is organized as follows. First, in section II, we describe the experimental and theoretical methods to be used. In section III, we then present our measurements of the reacted surfaces using AES, LEED, and TPD methods. We also present our DFT calculations of the adsorption energy and activation barrier for the reaction of these organosulfur molecules on Si(100), using a single-dimer cluster Si(100) model. The combination of theory and experiment provides insight into the adsorption and dissociation mechanisms of each organosulfur compound with Si(100). In addition, the similarity between the surface-reaction mechanism of the methyl sulfides and methylamines is discussed. Finally, section IV summarizes the essential findings of this paper.

## II. Experimental and Theoretical Methods

**Experimental Methods.** The experiments were performed in an UHV chamber equipped with a differentially pumped quadrupole mass spectrometer for temperature-programmed desorption (TPD), a hemispherical energy analyzer for Auger electron spectroscopy (AES), a low-energy electron diffraction (LEED) system, and an ion gun for sputter cleaning of the sample. The chamber had a typical base pressure of $1 \times 10^{-10}$ mbar, achieved with a 550 L $s^{-1}$ turbomolecular pump and a titanium sublimation pump.

The Si(100) samples (7.5 mm × 10.5 mm × 0.385 mm) were cut from *p*-type B-doped, 1−10 Ω cm resistivity silicon wafers (Virginia Semiconductors). The sample mounting and heating method have been detailed in prior studies.[25] Briefly, a patterned molybdenum-sheet, 0.025 mm-thick heater was sandwiched between two silicon crystals tightly clamped together by two tungsten clips. Uniform heating of the sample to a temperature above 1200 °C was achieved by passing current through this patterned, high-resistivity molybdenum heater. This heater was mounted on a liquid-nitrogen-cooled manipulator allowing cooling of the sample to the desired temperature. The sample temperature was measured by a K-type (chromel−alumel) thermocouple spot-welded to the molybdenum heater near the edge of the sample.

The Si(100) sample was cleaned, after its introduction into the UHV system, by repeated cycles of 2-keV $Ar^+$ sputtering at room temperature and subsequent annealing at 870 °C for 10 min and 910 °C for 3 min. The order and cleanliness of the surfaces were verified with LEED and AES, respectively. The Si(100) surfaces, thus treated, showed well-ordered (2 × 1) LEED patterns and were free of oxygen, sulfur, and carbon contamination, as confirmed by AES.

The following organosulfur compounds were used: $CH_3SH$ (99.5+%), $CH_3SCH_3$ (99+%), $CH_3SSCH_3$ (99+%), all from Aldrich, and $H_2S$ (99.5%), from Matheson. Both $CH_3SCH_3$ and $CH_3SSCH_3$ are liquid at room temperature and were further purified by repeated freeze−pump−thaw cycles, while the other compounds were used without further purification. The purity of the compounds was checked frequently by mass spectrometry. The Si(100) samples were exposed to the organosulfur compounds at room temperature by back-filling the chamber through a variable leak valve, which was not located in the line of sight of the sample surface. The exposure was calculated by multiplying the exposure time by the constant overall chamber pressure, measured by an ion gauge without gas-specific sensitivity calibration. In general, the experiments examined the variation in the AES signal over the full range of exposure. The values for exposure throughout this work are given in monolayer equivalents (MLE) unless otherwise specified. One monolayer equivalent is equal to an exposure corresponding to the surface atomic density of Si(100) ($6.78 \times 10^{14}$ atoms/$cm^2$).[23] At 300 K, 1 MLE of $CH_3SSCH_3$, $CH_3SCH_3$, $CH_3SH$, and $H_2S$ corresponds to an exposure of 3.3, 2.6, 2.3 and 2.0 langmuir, respectively.

The quadrupole mass spectrometer (QMS) was enclosed in a water-cooled shroud with a 3-mm-diameter aperture located in front of its ionizer. The sample was placed ∼2 mm away from this aperture during TPD measurements to ensure that only species desorbing from the central area of the prepared surface were detected. A linear temperature ramp of 2 °C $s^{-1}$ was used for all TPD measurements. TPD data were collected with a computer program capable of monitoring 10 mass-to-charge ratios, simultaneously.

The electron-beam energy used to obtain AES was 3000 eV with a current density of ∼0.03 $\mu$A/$mm^2$ at the surface. Under these conditions, AES signals generally remained unchanged, even after several AES measurement cycles, indicating electron-induced desorption was negligible. The Si(LVV) peak was routinely measured for each run and served as an internal standard or reference for both energy and intensity.

Throughout, AES measurements and LEED observations were made after heating the sample to specific temperatures. The procedure was, first, to heat using the linear 2 °C $s^{-1}$ heating rate. When the desired temperature was reached, the substrate heating was then abruptly stopped, and the sample was immediately allowed to cool to room temperature. This heating procedure allowed the surface composition to be prepared using a well-established thermal schedule and then probed at room temperature with LEED and AES.

**Theoretical Methods.** To understand the energetics of adsorption of our organosulfur precursors, we performed electronic structure calculations based on density functional theory (DFT) using a cluster model of the Si(100) surface. Gaussian 98W was used for the calculations.[27] In this work, a $Si_9H_{12}$ one-dimer cluster was used to model the (2 × 1) surface.[12,13,28−34] The cluster is identical to that used in several previous studies and consists of two surface-layer Si atoms representing a single bare surface dimer and seven Si atoms representing three layers of subsurface bulk atoms.[12,13,28−34] The subsurface dangling bonds, due to the truncation of the bulk Si−Si bonds, are terminated by 12 hydrogen atoms to maintain a locally tetrahedral environment.[13,28,30] The $Si_9H_{12}$ cluster is the smallest unit that might realistically represent the (2 × 1) surface, although it neglects interactions with adjacent dimers.[29,33]

All calculations were carried out using the B3LYP hybrid density functional[35,36] and a double-$\xi$ Gaussian basis set with polarization functions and diffuse functions added to all heavy atoms (6-31+G*).[12,32,37,38] The optimization was performed without any geometric constraints or symmetry restrictions. The vibrational frequencies were calculated for each optimized geometry, using the same level of theory, to verify that it corresponded to a minimum on the potential energy surface or a saddle point, that is, a transition state. Limited mapping of the intrinsic reaction coordinates were done, such as in the vicinity of transition-state points.

For an optimized surface-reaction product, the net adsorption energy was obtained by subtracting the energy of the corre-

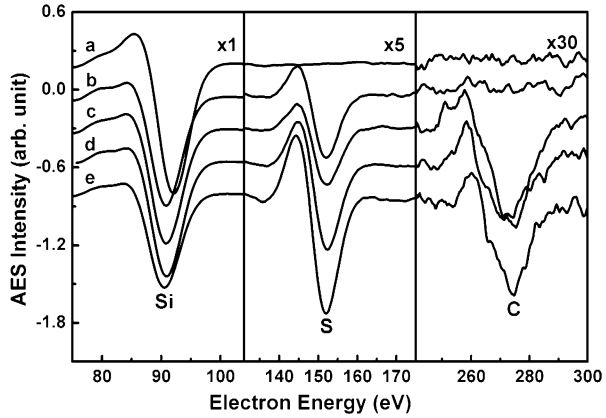


**Figure 1.** Auger spectra of the Si(LVV), S(LVV), and C(KLL) transitions for (a) clean Si(100) and after saturation exposure by (b) $H_2S$, (c) $CH_3SCH_3$, (d) $CH_3SH$, and (e) $CH_3SSCH_3$ at room temperature.

sponding optimized free precursor molecule and of the optimized free $Si_9H_{12}$ cluster from the total energy of this surface-reaction product. All energies reported were corrected by B3LYP/6-31+G* zero-point energies. It was found that zero-point energy corrections had a very small effect on the overall energies with a maximum correction of ~4 kJ/mol. Although the absolute values of the adsorption energies for the various adsorption configurations might have systematic errors, the relative values are expected to be accurate.[31,32]

### III. Results and Discussion

**1. Comparative Measurements of the Surface Auger Spectra.** Auger electron spectroscopy was used to study coverage-dependent adsorption of the four organosulfur compounds on Si(100)-(2 × 1) at room temperature. All Auger spectra were recorded in the d$N(E)$/d$E$ mode. Quantitative comparison between Auger spectra was conducted by normalizing the clean Si(LVV) peak-to-peak intensity for every experiment to eliminate the influence of sample position and drifts in electron beam current. The three most intense Auger lines for silicon, sulfur, and carbon, that is, Si(LVV) (92 eV), S(LVV) (152 eV), and C(KLL) (272 eV), were monitored during all AES measurements.

Figure 1 shows representative Auger Si(LVV), S(LVV), and C(KLL) spectra from Si(100) following saturating exposure to $CH_3SSCH_3$, $CH_3SCH_3$, $CH_3SH$, and $H_2S$. In addition, for comparison, the Auger spectra of clean Si(100) is also shown in Figure 1. For each of the four molecules, the Si(LVV) Auger lines are shifted to lower energies, by ~1.2 eV, relative to that on the bare Si(100) surface, thus indicating Si−S bond formation; S, being more electronegative than Si, shifts the Si(LVV) peak position to lower energy.[25] Saturation exposure was determined for each organosulfur molecule by observing the change in the Auger signal with coverage; saturation was judged to occur when the change in AES intensity with increasing exposure ceased. Notice that the saturation coverage of each molecule has a distinctive sulfur Auger intensity. In one case, that is, for $CH_3SCH_3$ and $H_2S$, these intensities are almost identical in magnitude.

The surface Auger signal was then used to measure the dependence of coverage on exposure. An example, for the case of dimethyl disulfide, is shown in Figure 2, which displays the dependence of the Auger intensity of the S(LVV) and Si(LVV) transitions and their ratio, S(LVV)/Si(LVV), upon exposure to $CH_3SSCH_3$ at room temperature. The data in Figure 2 show both the increasing S(LVV) signal, from sulfur in $CH_3SSCH_3$,

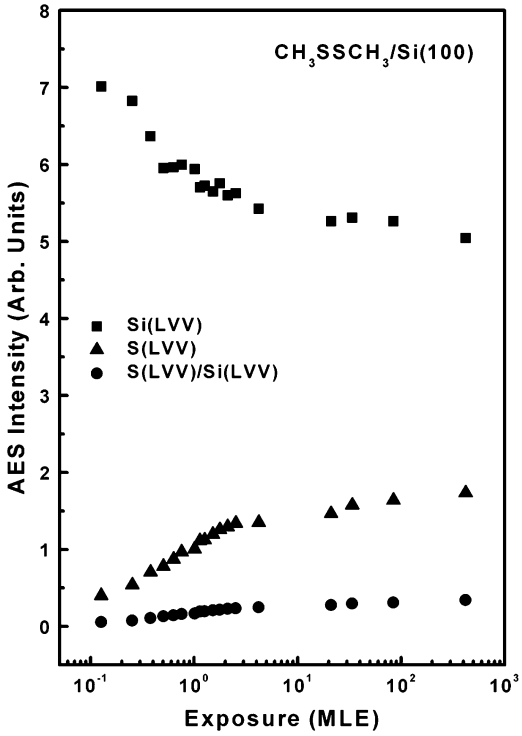


**Figure 2.** Auger peak intensity of the S(LVV) and Si(LVV) transitions and the ratio of S(LVV)/Si(LVV) transitions as a function of $CH_3SSCH_3$ exposure on Si(100) at room temperature.

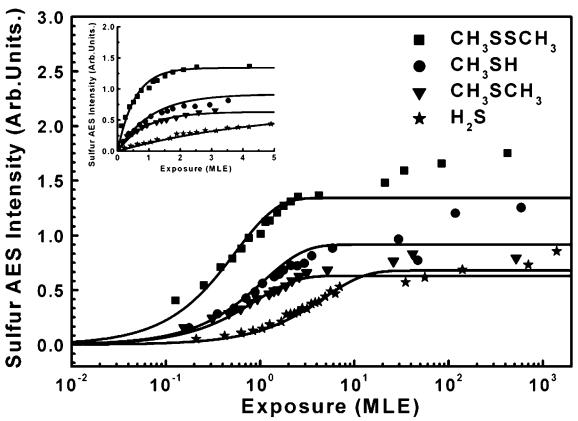


**Figure 3.** S(LVV) Auger peak intensity as a function of $CH_3SSCH_3$, $CH_3SCH_3$, $CH_3SH$, and $H_2S$ exposure on Si(100) at room temperature. The solid lines show the curves used to extract the initial sticking coefficient. The inset shows the enlarged view of the AES data at low exposure.

and the corresponding decreasing Si(LVV) signal as the Si(100) surface is covered with adsorbate. Notice that the sulfur Auger signal saturates for exposures above 10 MLE, a value also corresponding to saturation of the decrease in the Si Auger signal. A similar exposure variation in the Auger spectra has been observed for each of the organosulfur compounds on Si(100).

Figure 3 displays the exposure dependence of the S(LVV) Auger peak intensity for each of our four molecular species. The figure shows that each species has a characteristic saturation coverage, where the saturation coverage, $\theta_S$, is defined here as the number of the adsorbed organosulfur molecules per surface Si atom. This characteristic saturation coverage simply reflects the fact that the S(LVV) Auger signal is proportional to the sulfur surface concentration. Because the saturation coverage of $H_2S$ on clean Si(100)-(2 × 1) is known to be 0.5 ML,[23,25] $H_2S$ was used to calibrate the S coverage in monolayers for

**TABLE 1: The Measured Saturation Coverage, $\theta_S$,[a] Initial Sticking Probability, $S_0$, and the Ratio of the S(LVV)/C(KLL) Auger Intensity, $I_S/I_C$**

| species | $\theta_S$ | $S_0$ | $I_S/I_C$ |
|---|---|---|---|
| $CH_3SSCH_3$ | 0.49 | 0.90 | 8.77 |
| $CH_3SH$ | 0.68 | 0.64 | 7.78 |
| $CH_3SCH_3$ | 0.46 | 0.52 | 3.53 |
| $H_2S$ | 0.50[b] | 0.11 | *c* |

[a] The estimate of the errors in $\theta_S$ is ~0.05 ML. [b] References 23 and 25. [c] Not applicable.

our experiments. The saturation coverage of other organosulfur compounds adsorbed on Si(100) can thus be determined by comparing the S(LVV) Auger signal from the organosulfur-exposed Si(100) with that from a Si surface saturated by $H_2S$, both under identical experimental conditions. This comparison can be made more reliable by normalizing the signal to the clean-surface Si(LVV) Auger intensity, measured prior to each organosulfur exposure. Using this procedure, we determined the values of saturation coverage for adsorption of $CH_3SSCH_3$, $CH_3SCH_3$, and $CH_3SH$ to be 0.49, 0.46, and 0.68, respectively, as shown in Table 1. This result suggests that for adsorption of each organosulfur compound, except $CH_3SH$, each adsorbed molecule fills two Si surface sites, corresponding to one Si dimer.

It is possible to use the uptake data shown in Figure 2 to obtain a relative measure of the initial sticking coefficient for each organosulfur compound. To make this estimate, the initial slope of each curve is first fit to a simple first-order Langmuir isotherm. In particular, we can then express the coverage dependence of the S and Si Auger signals:[39]

$$I_{Si}(\theta) = I_{Si}^{clean}(1 - \theta) + I_{Si}^{ad}\theta \quad (1)$$

$$I_S(\theta) = I_S^{ad}\theta \quad (2)$$

where $\theta$ is surface coverage and $I_{Si}^{clean}$ and $I_{Si}^{ad}$ represent the Auger signal from a clean Si surface and a Si surface covered by adsorbates, respectively. The coverage dependence of the sticking probability, $S$, is then described by

$$S = \frac{d\theta}{dL} = S_0(1 - \theta/\theta_S) \quad (3)$$

where $L$ is the exposure, $\theta_S$ represents the saturation coverage, and $S_0$ is the initial sticking probability, given by the initial slope of the uptake curve. The fit of the experimental data with first-order Langmuir kinetics is shown in Figure 3. These values, summarized in Table 1, show that the initial sticking probability for $CH_3SSCH_3$, $CH_3SH$, $CH_3SCH_3$, and $H_2S$ are ~0.90, 0.64, 0.52, and 0.11, respectively. Note that, as mentioned in the previous section, the values of exposure used above are based on uncorrected ion-gauge readings. In fact, ion-gauge sensitivities are not known for most of the molecular species used in this paper. In general, because the sensitivity scales with the polarizability of the gas molecules,[40] the corrected pressures will be lower than the measured values; that is, the calculated initial sticking coefficients are an underestimate of readings based on a calibration to $N_2$, which has a low polarizability. However, the central point to our measurement of sticking probabilities is to enable a qualitative comparison between the adsorption probabilities of the various organosulfur molecules. Because the variation in polarizabilities is relatively modest, that is, a factor of ~1.4−2.8, our comparison should provide a reasonable qualitative comparison.

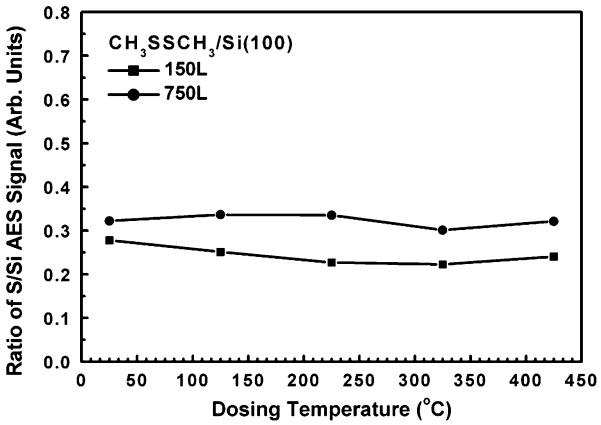


**Figure 4.** The ratio of S(LVV)/Si(LVV) Auger peak intensity versus substrate temperature during $CH_3SSCH_3$ exposure. The data show that saturation coverage is essentially independent of dosing temperature from room temperature to 450 °C.

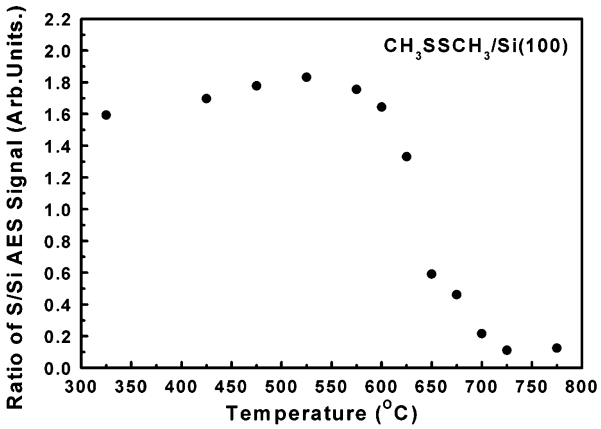


**Figure 5.** S(LVV)/Si(LVV) Auger peak intensity measured for Si(100) exposed to 7.5 L of $CH_3SSCH_3$ as a function of the surface temperature.

Also included in Table 1 is the ratio of the S(LVV) to C(KLL) Auger peak-to-peak intensity, $I_S/I_C$, for each organosulfur compound adsorbed on Si(100) at saturation exposure. These ratios follow the ratio expected on basis of the molecular stoichiometry, for example, the $I_S/I_C$ for $CH_3SSCH_3$ and $CH_3SH$ are nearly equal, reflecting the fact that their ratio of sulfur to carbon atoms is identical.

The dependence of the ratio of the S(LVV)/Si(LVV) Auger signal on substrate temperature, as measured with a saturated $CH_3SSCH_3$-exposed surface, was also investigated. The results are displayed in Figure 4 for two different values of saturation flux. The figure shows that the ratio of the S/Si Auger signal is constant for deposition temperatures between room temperature and 425 °C, indicating that the saturation coverage is nearly the same over the range of substrate exposure temperatures examined here.

Auger measurements were also made after thermal treatment of the sulfur-exposed surface following a 7.5 L $CH_3SSCH_3$ exposure of Si(100) at room temperature. The measurements were made after first heating the $CH_3SSCH_3$-saturated surface to a specified temperature and then cooling to room temperature, as described in the Experimental and Theoretical Methods section. Figure 5 shows the ratio of S(LVV) to Si(LVV) Auger peak intensity versus temperature. A careful examination reveals that both the S and Si signals (not shown here), as well as the S/Si ratio slightly increased after heating to temperatures below ~500 °C. An increase of both the Si-substrate and the S-adsorbate Auger signal intensities after thermal treatment was

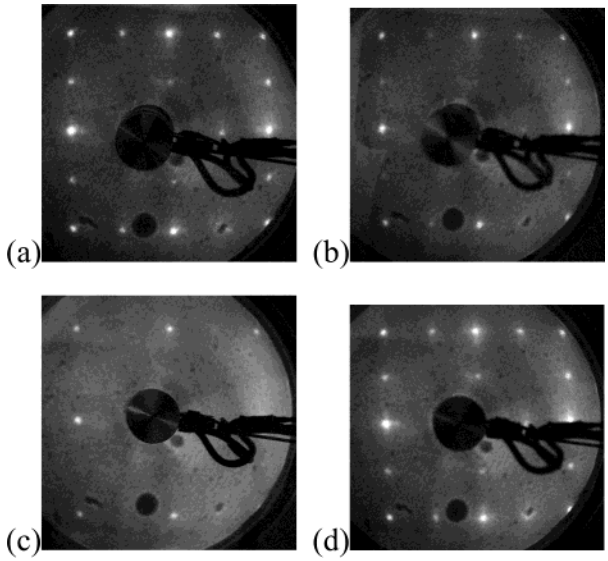


**Figure 6.** LEED patterns obtained at 55 eV from $CH_3SH$/Si(100) at room temperature: (a) clean Si(100)-(2 × 1); (b) a mixture of (1 × 1) and (2 × 1) patterns resulting from the adsorption of $CH_3SH$ on Si(100) at a coverage of ~0.25 ML; (c) complete conversion of (2 × 1) to (1 × 1) upon saturation by $CH_3SH$; (d) recovered (2 × 1) after annealing surface shown in panel panel c at 700 °C.

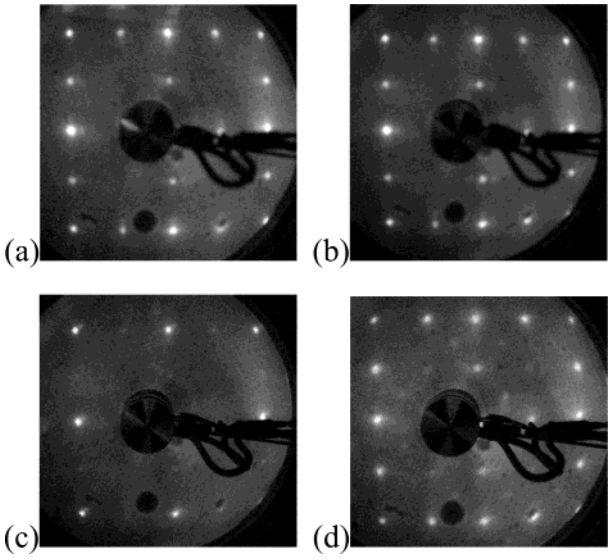


**Figure 7.** LEED patterns obtained at 55 eV from $CH_3SSCH_3$/Si(100) at room temperature: (a) clean Si(100)-(2 × 1); (b) (2 × 1) pattern resulting after saturation exposure of $CH_3SSCH_3$ on Si(100); (c) conversion of (2 × 1) to (1 × 1) after subsequent annealing of panel b at $T$ = 400 °C; (d) mixed Si (2 × 1) and c(4 × 4) obtained after further annealing at 700 °C.

also observed in our previous investigation of the $H_2S$/Si system and explained by a temperature-mediated increase in surface order. In addition, Figure 5 also shows that $CH_3SSCH_3$ forms a strongly bound complex on Si(100) up to a substrate temperature of 500 °C. Further heating above 525 °C reduced the surface sulfur, as shown in Figure 5. The disappearance of the Auger signal is in accord with other observations of S adsorbed on Si(100).[25,41] In those experiments, loss of surface sulfur signal was attributed to atomic sulfur diffusing into the bulk of the silicon.

**2. Low-Energy Electron Diffraction Measurements of the Reacted Silicon Surface.** *Introduction.* Low-energy electron diffraction (LEED) measurements were made after exposing Si(100) to $CH_3SSCH_3$, $CH_3SCH_3$, and $CH_3SH$. For each species, the variation of the room-temperature LEED patterns was measured at several different exposures, from unexposed to saturation. Heating of each saturated surface was also examined. Interestingly, the observed LEED behavior of the $CH_3SSCH_3$-exposed surface differed from that of surfaces exposed to $CH_3SCH_3$ or $CH_3SH$. Note that LEED measurements were not made on an $H_2S$-exposed surface because work on this system had been done earlier in our laboratory and has been separately reported.[25] Briefly, our earlier LEED observations for $H_2S$/Si(100) showed that, at room temperature, the (2 × 1) periodicity remained even after saturation coverage.[25]

*$CH_3SCH_3$ and $CH_3SH$: Results and Discussion.* Our measurements of the LEED patterns of $CH_3SCH_3$- and $CH_3SH$-exposed Si(100) showed a similar variation with changes in coverage and heating schedule. An example of this behavior for $CH_3SH$ is given in Figure 6. The LEED pattern for clean Si(100), Figure 6a, shows a well-defined (2 × 1) reconstruction at room temperature. Following exposure to methanethiol, see Figure 6b,c, the half-order spots become weaker and the integer-order spots become more intense, thus showing the transition of the (2 × 1) pattern to (1 × 1); at saturation exposure, the LEED pattern changes to a clear (1 × 1) configuration with a slight increase in background intensity. During subsequent heating of the $CH_3SH$-saturated sample, the (1 × 1) pattern remains well defined up to 400 °C (not shown). Upon further heating of the sample, the (1 × 1) pattern gradually diminishes and is replaced by a (2 × 1) pattern at ~700 °C; see Figure 6d. This (2 × 1) pattern then sharpens and intensifies with increasing temperature until ~900 °C.

A restoration of a reconstructed semiconductor surface to its original bulk-terminated surface, which is similar to that shown in Figure 6c, was observed after elemental sulfur deposition on Si(100)-(2 × 1) and Ge(100)-(2 × 1).[42,43] For example, Weser et al. found that S adsorption removes the (2 × 1) reconstruction to produce a (1 × 1) bulk-terminated S/Ge surface.[42] Later Papageorgopoulos et al. showed that adsorption of S at room temperature also caused an exposure-dependent change of Si(100)-(2 × 1) to its (1 × 1) phase.[43] This group suggested that the Si−S bond energy, which is greater than that of Si−Si, may be the driving force for the transition of the (2 × 1) to (1 × 1). In our experiments, the variation in the LEED patterns for a saturated $CH_3SCH_3$- and $CH_3SH$-dosed surface with the temperature of the Si substrate was identical to that observed in these earlier experiments. These results suggest that the strong Si−S interaction is apparently not affected by the presence of other coadsorbed species such as $CH_3$ or H for $CH_3SCH_3$- and $CH_3SH$-exposed Si(100), respectively.

*$CH_3SSCH_3$: Results and Discussion.* As mentioned earlier in this section, a $CH_3SSCH_3$-exposed surface showed a different LEED behavior than that exposed to $CH_3SCH_3$ and $CH_3SH$. The LEED results for the $CH_3SSCH_3$-dosed surface are shown in Figure 7. Figure 7a shows a clean Si(100)-(2 × 1) pattern at room temperature. After a saturation exposure of the clean surface to $CH_3SSCH_3$ at room temperature, the (2 × 1) LEED pattern remains clear and intense as shown in Figure 7b, suggesting that dimer bonds remain intact in the presence of adsorbed $CH_3SSCH_3$; see discussion below. This unchanged (2 × 1) LEED pattern is also consistent with our AES measurements, which showed that one $CH_3SSCH_3$ molecule adsorbs per Si−Si dimer for a saturated surface. The retention of the (2 × 1) LEED pattern on the $CH_3SSCH_3$-saturated surface and its relation to the possible adsorption geometries will be discussed further in the next section. In addition, Figure 7c shows that subsequent heating of the $CH_3SSCH_3$-saturated surface to 400

°C for 2 min causes the (2 × 1) LEED pattern to change to (1 × 1). After further heating of the sample to 700 °C for 2 min, the LEED pattern changes from (1 × 1) to a mixed (2 × 1)/c(4 × 4) pattern as shown in Figure 7d. After increasing the surface temperature to between 700 and 900 °C, the surface changes back to the reconstructed (2 × 1), not shown here.

The appearance of the c(4 × 4) phase on Si(100) has been previously observed by others, and its origin has been extensively discussed in the literature.[44−46] In at least one case, this phase was observed on a sulfur-exposed surface. In particular, Moriarty et al. reported that annealing of S-covered Si(100)-(2 × 1) at 325 °C led to the appearance of a mixed c(4 × 4) and (2 × 1) surface reconstruction,[47] which persisted up to temperature ∼700 °C. In our case, it is highly unlikely that the appearance of the c(4 × 4) phase is related to the presence of sulfur because, at the temperature for which we observe the phase, that is, 700 °C, sulfur is known to diffuse into the Si bulk. In addition, other groups have obtained the c(4 × 4) reconstruction merely by annealing the Si(100) surface in UHV.[44−46] Careful studies[44−46] have shown that these observations were related to the presence of intentional or adventitious carbon on the surface. For example, Nörenberg et al. used STM, AES, reflection high-energy electron diffraction (RHEED), and LEED to find a c(4 × 4) reconstruction mixed with (2 × 1) patches after annealing Si(100)-(2 × 1) at 500 °C for several hours in UHV. AES measurements showed that the c(4 × 4) reconstruction could be attributed to the presence of carbon.[46]

There is no universal agreement about the atomic arrangement in the c(4 × 4) reconstruction seen when carbon is present. Nörenberg et al. suggested a missing-dimer model, in which dimer vacancies are combined with C atoms sitting in the fourth layer.[46] Their results also support the suggestion, presented by Miki et al., that a stress field induced by the impurities in subsurface locations is responsible for the c(4 × 4) phase.[44,48] Other interpretations, which consider near-surface stress, have been advanced in other experiments.[49,50] Considering the similarity between our LEED patches of the (2 × 1) and c(4 × 4) and those of Nörenberg et al., as well as our observations of appreciable carbon on the $CH_3SSCH_3$-saturated surface at 700 °C, suggests that the appearance of our c(4 × 4) phase is due also to stress induced by near-surface carbon impurities.

**3. Temperature-Programmed Desorption Spectra.** Temperature-programmed desorption measurements were made for Si(100) saturated with the four organosulfur compounds. Their thermal desorption behavior can help identify the surface-bound species and possible surface reaction pathways. Figure 8 shows a comparison of $H_2$ and $CH_3$ desorption spectra for four Si(100) samples saturated with each of the organosulfur species at room temperature. A large number of possible desorption species were monitored during our TPD measurements including S, $S_2$, SiS, SH, $H_2S$, $CH_3S$, $CH_3SH$, $CH_3SCH_3$, $CH_3SS$, and $CH_3SSCH_3$, as well as the hydrocarbon fragments $CH_3$, $CH_4$, $C_2H_2$, $C_2H_4$, $C_2H_5$, and $C_2H_6$. However, only desorption of $H_2$ from a Si surface saturated with $H_2S$ and of $H_2$ and $CH_3$ from a Si-surface saturated with methyl-containing compounds were observed. No SiS species were observed within the detection limits of our mass spectrometer. In previous work in our laboratory, it was shown that, instead of desorbing from the surface, sulfur diffuses into the Si bulk during heating.[25] It was suggested that, in the case of sulfur, the diffusion barrier is lower than the energy required to break the Si back-bonds.[25] Note also that, although minor desorption of $C_2H_x$ species have been previously observed in the TPD measurements of methyl-covered Si(100) surfaces,[51] no evidence of any such $C_2H_x$ fragments were seen here. However, the possibility that our lack of observation of these species is simply because the signals of these minor desorption channels are beyond the detection limits of our mass spectrometer cannot be ruled out.

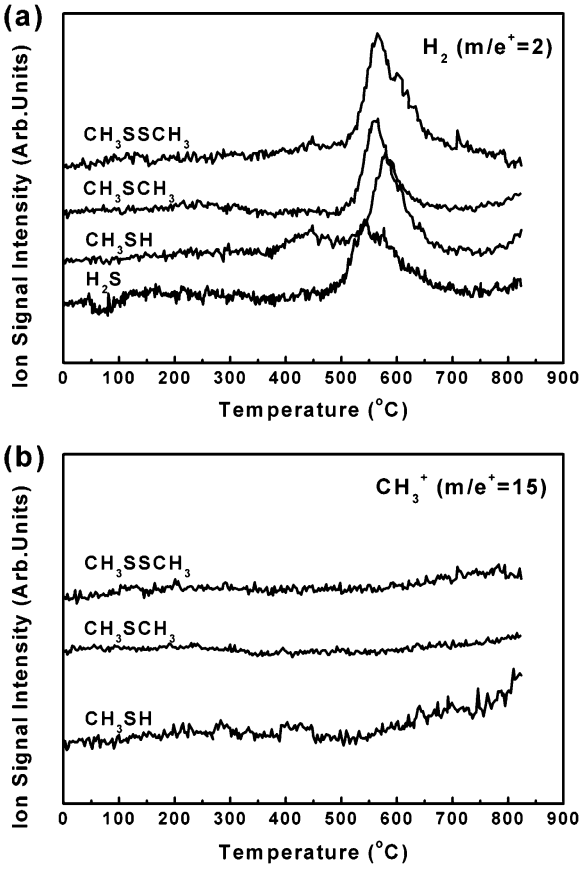


**Figure 8.** $H_2$ TPD spectra (a) for $m/e = 2$ and $CH_3$ TPD spectra (b) for $m/e = 15$ from Si(100) saturated with several organosulfur precursors at room temperature.

In particular, as shown in Figure 8, only one $H_2$ desorption peak at ∼545 °C was observed for the $H_2S$-saturated surface at room temperature, indicating the presence of a single desorption channel. A comparison with $H_2$-desorption spectra from an atomic-hydrogen-dosed Si(100) surface shows that this feature comes from the surface monohydride phase.[25] The ∼20 °C shift to higher temperature in Figure 8 compared to that on a H-exposed surface has been observed previously[25] and attributed to a perturbation of the Si−H bond energy due to the presence of adsorbed sulfur on the Si surface.

As shown in Figure 8 desorption of $H_2$ was also observed for the Si(100) surface saturated with $CH_3SSCH_3$, $CH_3SCH_3$, and $CH_3SH$. $H_2$ desorbed at 566−576 °C for these saturated surfaces; in addition, in the case of $CH_3SH$, an additional feature was also seen at ∼440 °C. The peak temperature of this small hydrogen-desorption feature is within ∼17 °C of that for temperature-programmed desorption of the dihydride phase on a heavily hydrogenated Si surface[25,52] and even closer, that is, ∼12 °C, if the dihydride phase is formed by exposure to $H_2S$ at low temperature. Thus, appearance of this feature is most likely due to the formation of surface dihydride, which originates from excess adsorbed H from $CH_3SH$ decomposition at high exposure, as discussed in the next section.

As shown in Figure 8, the $H_2$ desorption temperature for the surface saturated with methyl-containing organosulfur precursors is 21−31 °C higher than that for the surface saturated with $H_2S$. This result suggests that the $H_2$ desorption channel has a

different origin for surfaces saturated with $H_2S$ than those saturated with methyl-containing molecules. Note that because all four precursors contain sulfur, the shift in $H_2$ desorption temperature is unlikely to be due to interaction with adsorbed sulfur, as mentioned above. Instead, because the methyl C−H bond is stronger than the Si−H bond, the $H_2$ desorption features observed in the TPD spectra of Si(100) surface saturated with those methyl-containing organosulfur precursors most likely originate from the dehydrogenation of the methyl groups on the surface.[53] This result implies that upon adsorption those methyl-containing organosulfur precursors do not undergo C−H bond cleavage and the methyl groups remain intact in the adsorbed state. Thus upon adsorption the possible dissociation channels are consistent with S−S or S−C bond breaking or both for $CH_3SSCH_3$, S−H or S−C bond breaking or both for $CH_3SH$, and S−C bond breaking for $CH_3SCH_3$.

**4. Density Functional Theory Calculations.** Calculations, described below, were carried out to examine the energetics of potential chemisorption routes for each molecule. In addition, a limited number of calculations of the reaction kinetics were done for certain adsorption processes. Recall that because of the size of our computational system, energetics were only calculated for reactions with a single-Si-dimer cluster.

*Hydrogen Sulfide ($H_2S$).* As mentioned in section III, the reaction of $H_2S$ with silicon surfaces was used as a benchmark system for both our theoretical and earlier-mentioned experimental studies. Energetics were calculated for two dissociation channels. In the first, partial dissociation occurs via scission of the S−H bond to form H and S−H, each bound to a separate Si atom of a surface dimer. In the second, $H_2S$ fully dissociates into S and two H atoms with the S bridge-bonded between each of the Si dimer atoms and each H atom also bonded to these same Si atoms. The calculated adsorption energies for these two bonding configurations were found to be 241.8 and 304.6 kJ/mol, respectively, giving an energy difference of 62.8 kJ/mol between the two channels. This value is in good agreement with recent calculations by Çakman and Srivastava,[54] also using density functional computation but with a periodic slab geometry. These authors optimized each of the two adsorption geometries for the two channels and found that the adsorption geometry corresponding to full dissociation was 56.9 kJ/mol lower in energy than that corresponding to partial dissociation. The fact that our calculations are in good agreement with this work provides benchmarking for our procedure.[55]

*Dimethyl Disulfide ($CH_3SSCH_3$).* Two possible dissociation channels, namely, S−S and S−C bond cleavage, were investigated for adsorption of $CH_3SSCH_3$ on Si(100)-(2 × 1): cleavage of the S−S bond leading to the formation of two methyl thiolates (S−$CH_3$), which then sulfur bond to each of the two Si-dimer atoms, and S−C bond cleavage to form $CH_3$−S−S and $CH_3$, which then sulfur and carbon bond to the dimer, respectively. Both mechanisms are consistent with our AES results, which provide evidence for the formation of Si−S bonds and the formation of 0.5 ML coverage at saturation by $CH_3SSCH_3$.

Figure 9 shows the optimized geometries for these two adsorption mechanisms. The calculated adsorption energies, as shown in Figure 9, show that both reactions are exothermic with adsorption energies of 307.9 and 270.3 kJ/mol for processes involving S−S and S−C bond cleavage, respectively. This result shows that adsorption involving S−S scission is thermodynamically more favorable than that via S−C bond scission. While a transition-state search was not performed for the two dissociation pathways, the high reactivity of $CH_3SSCH_3$ with Si(100) at room

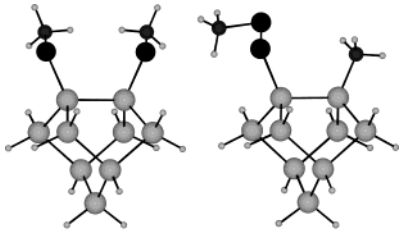


**Figure 9.** Optimized adsorption geometries for (a) S−S bond dissociation and (b) S−$CH_3$ dissociation of $CH_3SSCH_3$ on a $Si_9H_{12}$ cluster. The black atoms are S; the dark gray atoms are C; the large and small light-gray atoms are Si and H, respectively.

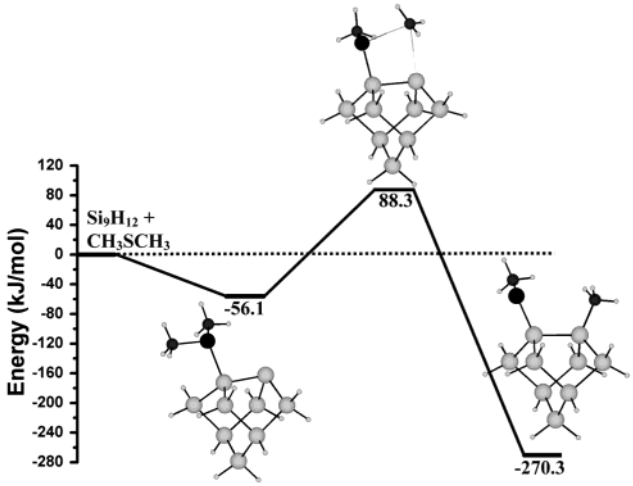


**Figure 10.** Potential-energy diagram and optimized structures for reaction of $CH_3SCH_3$ with a $Si_9H_{12}$ cluster via S−C bond scission. The black atoms are S; the dark gray atoms are C; the large and small light-gray atoms are Si and H, respectively.

temperature, for example, a near-unity (0.9) initial sticking probability, suggests that the barrier for one or both of the reactions is below the vacuum level. In this regard, the adsorption geometry shown in Figure 9a for S−S bond cleavage would appear to be more favored because it is more energetically favorable. In addition, note that S−S bond cleavage has been observed for adsorption of disulfide functional groups on gold surfaces.[56−59] Scission of the S−S bond in other disulfide compounds has also been observed on Si(100). For example, Coulter et al. have recently showed that diphenyl disulfide bonds to Si(100) via scission of the S−S bond to form two sulfur−phenyl moieties, which then sulfur bond to the Si surface.[38] Although the possibility of dissociation via S−C bond cleavage cannot be completely dismissed, it is most likely that room-temperature adsorption of $CH_3SSCH_3$ proceeds primarily via S−S bond cleavage, that is, by forming surface Si−S−$CH_3$ moieties. The adsorption geometry shown in Figure 9a is also consistent with the preservation of a (2 × 1) LEED pattern after $CH_3SSCH_3$ exposure.

*Dimethyl Sulfide ($CH_3SCH_3$).* Chemisorption of $CH_3SCH_3$ on Si(100) via S−$CH_3$ dissociation to give surface S−$CH_3$ and $CH_3$ groups, shown schematically in Figure 10, was investigated. Our calculations show that $CH_3SCH_3$ initially molecularly adsorbs on the lower Si atom of the tilted surface dimer. The Si−S bond length for this molecular complex is 2.37 Å; this bond is much longer than the 2.18 Å Si−S bond calculated for the dissociative adsorption products of $CH_3SSCH_3$ and $CH_3SCH_3$. This result is characteristic of dative bonding in the adsorption complex; similar cases have been reported for DFT calculation for amines and $CH_3OH$ on Si(100).[10,12−14] Our

calculation shows that the adsorption energy for this molecular complex is 56.1 kJ/mol. The adsorption energy of the final dissociation products is −270.3 kJ/mol, while the activation barrier is +88.3 kJ/mol with respect to the vacuum level. Thus, although S−$CH_3$ dissociation is thermodynamically favorable, the activation barrier for dissociation is sufficiently large that bond scission is not kinetically favored at the room temperature. Consequently, our calculations indicate that $CH_3SCH_3$ will bind to the surface molecularly intact at room temperature.

Specifically, our calculations, which use a one-dimer cluster model, show that the molecularly adsorbed $CH_3SCH_3$ will not dissociate into Si−$CH_3$ and Si−S−$CH_3$ species on the same dimer. However, obviously this calculation cannot rule out the possibility of the initially molecularly adsorbed $CH_3SCH_3$ dissociating through the S−C bond cleavage on *adjacent* dimers. In fact, dissociation on adjacent Si dimers is seen for the case of $H_2S$. To resolve this issue, it would be useful to perform calculations for a two-dimer cluster.

Note, however, that there is as yet no experimental evidence to support or disprove the occurrence of molecular desorption. While TPD data do not show evidence of intact $(CH_3)_2S$ desorbing from the surface, this absence could easily be a result of surface dissociation before intact desorption could occur; in addition, AES measurements are in accord with either an intact or disassociated molecule. Unfortunately, the LEED behavior for the $CH_3SCH_3$-exposed Si(100) surface is also not conclusive in this regard. As mentioned in the text, a (2 × 1) LEED pattern was seen for a range of coverage of up to ∼0.25 ML of $CH_3SCH_3$, a result consistent with either intact molecular adsorption or various dissociative adsorption products. However, the origin of the conversion of (2 × 1) to (1 × 1) at higher coverage, that is, ≥0.25 ML of $CH_3SCH_3$, is less obvious. One possible explanation is that at high coverage surface rearrangement may also occur, breaking Si dimers in a manner analogous to the $H_2S$[25] and H system[52] or the $CH_3SH$ system, as will be discussed in somewhat more detail in the section that follows.

*Methanethiol ($CH_3SH$).* Two possible chemisorption pathways, that is, S−H or S−C bond cleavage, were investigated for $CH_3SH$. The S−H bond scission forms surface Si−H and Si−S−$CH_3$ species, while S−C bond cleavage leads to the formation of surface Si−S−H and Si−$CH_3$ species. Different transition states were examined to determine the possible mechanisms and barriers for these two reactions. Figure, 11a,b shows the potential-energy diagrams for the three stages of S−H and S−C bond scission, respectively. The energies for those stages are also shown in Figure 11. Our calculations show that S−H bond dissociation in $CH_3SH$ occurs via a molecularly absorbed state, which has an adsorption energy of 38.1 kJ/mol. The transition state for the S−H dissociation is located 27.2 kJ/mol below the vacuum level, so overall, dissociation is 243.9 kJ/mol exothermic. In comparison, the calculated dissociation reaction for S−$CH_3$ is 276.6 kJ/mol exothermic, while the activation barrier is 89.1 kJ/mol above the vacuum level. Thus, for $CH_3SH$, although the S−H dissociation pathway is less energetically favorable than that for S−C bond, the S−H dissociation pathway is kinetically favored because its activation energy is below the vacuum level while the activation barrier for the S−C dissociation pathway is above the vacuum level.

Thus, our calculations suggest that the reaction of $CH_3SH$ with Si(100) should proceed via S−H bond scission to form surface S−$CH_3$ and H species. This result is consistent with recent theoretical calculations for the adsorption of $CH_3OH$ on Si(100)[10] and experimental observations of the adsorption of $CH_3OH$ on porous Si[60] and Si(111).[61] Our result is also

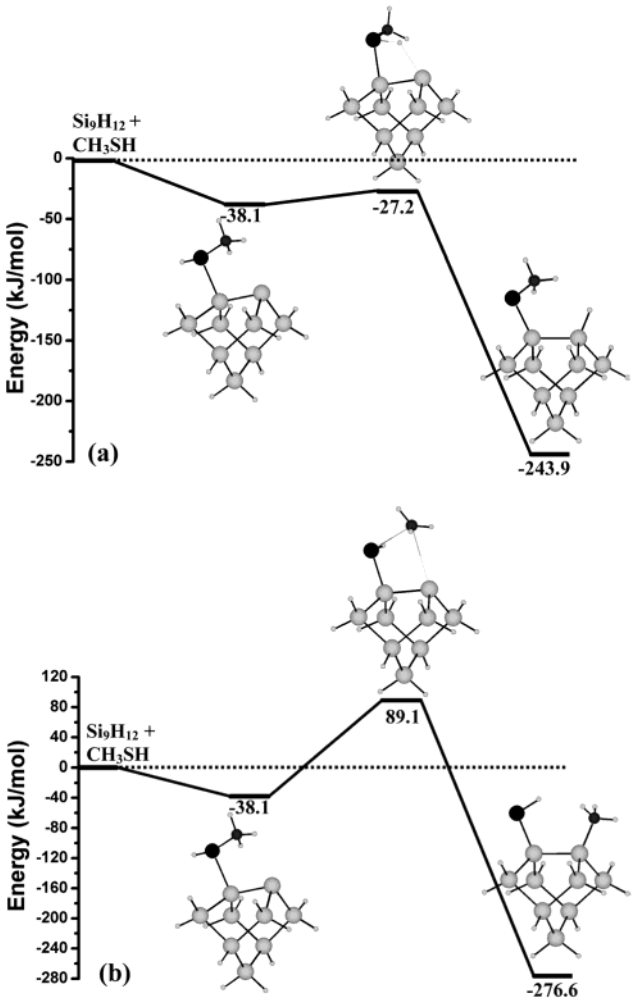


**Figure 11.** Potential-energy diagrams and optimized structures for (a) S−H dissociation pathway and (b) S−$CH_3$ dissociation pathway for $CH_3SH$ on a $Si_9H_{12}$ cluster. The black atoms denote S; the dark gray atoms denote C; the large and small light-gray atoms denote Si and H, respectively.

consistent with the relatively high initial sticking probability (0.64) of $CH_3SH$ molecules, which would follow from the fact that S−H bond dissociation has no barrier and is exothermic. However, our experimental observation of a 0.68 ML $CH_3SH$ saturation coverage, obtained from AES measurements, along with its (1 × 1) LEED pattern cannot be reconciled with the adsorption product formed through S−H bond dissociation, as shown in Figure 11. A process involving S−H scission would be expected to yield a (2 × 1) LEED pattern and 0.5 ML saturation coverage, neither of which is observed in our experiments. This discrepancy between theoretical calculations and experiment may be simply due to a process in which, at high exposure, $CH_3SH$ reacts with other surface adsorbates. This second-order process could result in additional surface rearrangement. This type of behavior is relatively common; for example, it has been observed in the adsorption of elemental S[43] and $H_2S$[25] on Si(100). In addition, the extra dihydride feature seen in the TPD spectra of the $CH_3SH$-saturated Si surface may also be due to such surface rearrangement. For the dihydride to form requires the breaking of the dimer bonds. In that case a (1 × 1) LEED pattern for the $CH_3SH$-saturated Si surface would be expected because that pattern would reflect the periodicity of substrate surface layer. To clarify whether such a rearrangement mechanism occurs in the $CH_3SH$/Si system and to

determine the corresponding exact adsorption geometry, further investigation is needed.

**5. Comparison with Other Systems.** The Si(100) reconstructed surface exhibits a Lewis acid−base chemistry, which might be expected to apply to several classes of molecular adsorbates. In particular, each Si surface dimer tilts out of the surface permitting transfer of electron density from the "down" atom to the "up" atom of the dimer.[62] Thus the "down" atom has a small positive charge relative to the "up" atom, causing the former to be electrophilic and the "up" atom to be nucleophilic.[4,28,63,64]

In this connection, our DFT cluster calculations of the reactions of methyl sulfides on Si(100) show clear similarities with recent investigations of methylamine reactions on Si(100).[12−14] First, Mui et al.[13,14] have shown that the surface dissociation of methylamine and dimethylamine occurs preferentially via N−H rather than N−$CH_3$ bond scission. Similarly in the case of methyl sulfides, our results for $CH_3SH$ show that S−H bond dissociation is kinetically more favorable than S−$CH_3$ bond dissociation. Second, both trimethylamine and dimethyl sulfide adsorb molecularly on Si(100).

The electron-donor character of the N and S lone pairs play an important role in these common properties of methyl sulfides and methylamines on Si(100). In the case of the amines, Mui et al.[13,14] have shown that the interaction between the N lone pair and the electron-deficient down atom of the Si dimer leads to the formation of this molecularly adsorbed state. This interaction, which resembles a Lewis acid−base interaction, causes the amine to chemisorb via a dative-bonded intact molecule. This same group has also described the chemical origin of the selectivity of the N−H versus N−$CH_3$ dissociation for dissociative adsorption of methylamine and dimethylamine. Basically, they conclude that N−H dissociation mimics the transfer of a proton from the ammonium ion to the electron-rich "up" Si atom through a Lewis acid−base reaction, while the N−$CH_3$ dissociation pathway can be considered as a nucleophilic substitution reaction.

The sulfur lone pairs should also strongly interact with the Si dimer. For example, Coulter et al.[38] have suggested that the selective binding of the benzenethiol and diphenyl disulfide to a Si surface is due to this interaction. To the best of our knowledge, no previous systematic theoretical calculation of the energetics and kinetics for the adsorption of organosulfur compounds on Si(100) surface has been performed. Thus our calculations provide insight into the role of the interaction between the S lone pair and the buckled Si dimer in the reaction of organosulfur compounds with Si.

Finally, the reaction of those organosulfur compounds with *multiple* Si dimers has not been investigated in this work. However, note that nonlocal effects, which can be observed in multiple dimer clusters, do not appear to be substantial for the reaction of amines with Si(100) because calculations for amines using DFT and $Si_9H_{12}$ are in good agreement with experimental results.[12−14] In addition, Widjaja and Musgrave have studied nonlocal effects of $NH_3$ adsorption and dissociation on Si(100) surface with one, three, and five dimer clusters.[28,65] They found qualitative agreement between all cluster models for the energetics of the adsorption of $NH_3$ on Si(100). These results support the applicability of single-dimer cluster in our calculations of organosulfur compounds on silicon. Note, however, as discussed above, the dissociation involving neighboring dimers apparently is important for the case of $H_2S$.[23−26] Hence calculations using a two-dimer cluster model $Si_{15}H_{16}$ are underway in our lab.

## IV. Conclusions

This paper has used UHV probes in conjunction with ab initio theory to investigate the reaction of three methylated organosulfur molecules with Si(100) at room temperature. AES measurements show that each of these organosulfur compounds has a characteristic saturation coverage and reaction probability for chemisorption on Si(100). TPD studies indicate that methyl groups appear to remain intact after adsorption and dissociate only after heating to ∼440 °C. Our DFT calculations suggest that $CH_3SSCH_3$ dissociatively adsorbs on Si(100) via S−S bond cleavage, forming a S−$CH_3$ silicon-terminating species. This reaction scheme is consistent with our experimental results. For the case of dimethyl sulfide, our calculations indicate that $CH_3SCH_3$ molecularly adsorbs at room temperature because there is a barrier to dissociation on a single dimer. Investigation of more complex dissociation channels, including those involving multiple dimers, awaits a more extensive computational study. For adsorption of $CH_3SH$ on Si(100), our calculations indicate that $CH_3SH$ dissociatively adsorbs on Si(100) via S−H bond scission, forming surface S−$CH_3$ and H species. However, our experimental results are not consistent with such S−H bond dissociation. It is suggested that, at the high exposure conditions examined here, additional surface rearrangements due to the further reaction of $CH_3SH$ molecules with the initial adsorption products may occur. This high coverage reaction may explain the discrepancy between theoretical calculations and experimental results.

From a more general perspective, our DFT calculations show that the chemisorption mechanisms of methyl sulfides are similar to those found in recent studies of methylamines. The similarity of the electron-donor character of the N and S lone pairs appears to play an important role in the close resemblance of the dissociation mechanisms of the methyl sulfides and methylamines. Our investigation of the surface chemistry of these sulfides provides an opportunity to study the interactions between the S lone pairs and the buckled Si dimers in the reaction of the organosulfur compounds with silicon.

Finally, from the perspective of applications, understanding the adsorption chemistry of these organosulfur molecules on Si(100) also provides insight into the selection of organosulfur precursors for chemically controlled atomic-layer growth of sulfur-containing group II−VI semiconductors, for example, ZnS, on Si(100) surface at low temperature. For example, the dissociative adsorption of $CH_3SH$ and $H_2S$ involves formation of surface Si−H groups; these H atoms passivate the surface against further adsorption. Thus, in the presence of these precursors, removal of surface H becomes a major limit to material growth. In this case, adsorption will not yield 1.0 ML of surface sulfur, which is a prerequisite of layer-by-layer, self-limiting epitaxy. In the case of low-temperature adsorption of the $CH_3SCH_3$ and $CH_3SH$, surface S−$CH_3$ species will also form and be attached through the Si−S bond. These ligands will also block sites and prevent the formation of a full 1.0 ML of surface sulfur. Our results also indicate that $H_2S_2$, the molecular structure of which is analogous to that of $CH_3SSCH_3$, is a more suitable sulfur precursor for reactive epitaxy because the goal of 1 ML of sulfur can be achieved. In addition, the S−H termination would enable growth of the next Zn layer through the reaction of zinc precursor, for example, $(CH_3)_2Zn$, with surface S−H groups.

**Acknowledgment.** The authors thank Nick Camillone, Ming Han, Yi Luo, and Prof. Sean Casey for their helpful discussions and Prof. James Yardley for many hours of patient advice and

thoughtful discussion. They gratefully acknowledge the support of this work by NSF through a grant (Contract No. 0076461) and instrumentation support by the Department of Energy through a grant (Contract No. DE-FG02-90ER14104).

## References and Notes

(1) Yates, J. T. *Science* **1998**, *279*, 335.
(2) Wolkow, R. A. *Annu. Rev. Phys. Chem.* **1999**, *50*, 413.
(3) Hamers, R. J.; Coulter, S. K.; Ellison, M. D.; Hovis, J. S.; Padowitz, D. F.; Schwartz, M. P.; Greenlief, C. M.; Russell, J. N. *Acc. Chem. Res.* **2000**, *33*, 617.
(4) Bent, S. F. *J. Phys. Chem. B* **2002**, *106*, 2830.
(5) Appelbaum, J. A.; Baraff, G. A.; Hamann, D. R. *Phys. Rev. B* **1976**, *14*, 588.
(6) Hamers, R. J.; Tromp, R. M.; Demuth, J. E. *Phys. Rev. B* **1986**, *34*, 5343.
(7) Duke, C. B. *Chem. Rev.* **1996**, *96*, 1237.
(8) Ellison, M. D.; Hovis, J. S.; Liu, H. B.; Hamers, R. J. *J. Phys. Chem. B* **1998**, *102*, 8510.
(9) Casaletto, M. P.; Zanoni, R.; Carbone, M.; Piancastelli, M. N.; Aballe, L.; Weiss, K.; Horn, K. *Surf. Sci.* **2000**, *447*, 237.
(10) Kato, T.; Kang, S. Y.; Xu, X.; Yamabe, T. *J. Phys. Chem. B* **2001**, *105*, 10340.
(11) Mulcahy, C. P. A.; Carman, A. J.; Casey, S. M. *Surf. Sci.* **2000**, *459*, 1.
(12) Cao, X. P.; Hamers, R. J. *J. Am. Chem. Soc.* **2001**, *123*, 10988.
(13) Mui, C.; Wang, G. T.; Bent, S. F.; Musgrave, C. B. *J. Chem. Phys.* **2001**, *114*, 10170.
(14) Mui, C.; Han, J. H.; Wang, G. T.; Musgrave, C. B.; Bent, S. F. *J. Am. Chem. Soc.* **2002**, *124*, 4027.
(15) Suntola, T.; Hyvarinen, J. *Annu. Rev. Mater. Sci.* **1985**, *15*, 177.
(16) Yarmoff, J. A.; Shuh, D. K.; Durbin, T. D.; Lo, C. W.; Lapianosmith, D. A.; McFeely, F. R.; Himpsel, F. J. *J. Vac. Sci. Technol., A* **1992**, *10*, 2303.
(17) George, S. M.; Sneh, O.; Dillon, A. C.; Wise, M. L.; Ott, A. W.; Okada, L. A.; Way, J. D. *Appl. Surf. Sci.* **1994**, *82*−*3*, 460.
(18) Dillon, A. C.; Ott, A. W.; Way, J. D.; George, S. M. *Surf. Sci.* **1995**, *322*, 230.
(19) George, S. M.; Ott, A. W.; Klaus, J. W. *J. Phys. Chem.* **1996**, *100*, 13121.
(20) Luo, Y.; Slater, D.; Han, M.; Moryl, J.; Osgood, R. M. *Appl. Phys. Lett.* **1997**, *71*, 3799.
(21) Luo, Y.; Han, M.; Slater, D. A.; Osgood, R. M. *J. Vac. Sci. Technol., A* **2000**, *18*, 438.
(22) Widjaja, Y.; Musgrave, C. B. *Appl. Phys. Lett.* **2002**, *80*, 3304.
(23) Schroderbergen, E.; Ranke, W. *Surf. Sci.* **1990**, *236*, 103.
(24) Rezaei, M. A.; Stipe, B. C.; Ho, W. *J. Chem. Phys.* **1999**, *110*, 3548.
(25) Han, M.; Luo, Y.; Camillone, N.; Osgood, R. M. *J. Phys. Chem. B* **2000**, *104*, 6576.
(26) Romero, M. T.; Takeuchi, N. *Surf. Sci.* **2003**, *524*, 157.
(27) Frisch, M. J.; Trucks, G. W.; Schlegel, H. B.; Scuseria, G. E.; Robb, M. A.; Cheeseman, J. R.; Zakrzewski, V. G.; Montgomery, J. A., Jr.; Stratmann, R. E.; Burant, J. C.; Dapprich, S.; Millam, J. M.; Daniels, A. D.; Kudin, K. N.; Strain, M. C.; Farkas, O.; Tomasi, J.; Barone, V.; Cossi, M.; Cammi, R.; Mennucci, B.; Pomelli, C.; Adamo, C.; Clifford, S.; Ochterski, J.; Petersson, G. A.; Ayala, P. Y.; Cui, Q.; Morokuma, K.; Malick, D. K.; Rabuck, A. D.; Raghavachari, K.; Foresman, J. B.; Cioslowski, J.; Ortiz, J. V.; Stefanov, B. B.; Liu, G.; Liashenko, A.; Piskorz, P.; Komaromi, I.; Gomperts, R.; Martin, R. L.; Fox, D. J.; Keith, T.; Al-Laham, M. A.; Peng, C. Y.; Nanayakkara, A.; Gonzalez, C.; Challacombe, M.; Gill, P. M. W.; Johnson, B. G.; Chen, W.; Wong, M. W.; Andres, J. L.; Head-Gordon, M.; Replogle, E. S.; Pople, J. A. *Gaussian 98*, revision A.14; Gaussian, Inc.: Pittsburgh, PA, 1998.
(28) Widjaja, Y.; Mysinger, M. M.; Musgrave, C. B. *J. Phys. Chem. B* **2000**, *104*, 2527.
(29) Konecny, R.; Doren, D. J. *Surf. Sci.* **1998**, *417*, 169.
(30) Hall, M. A.; Mui, C.; Musgrave, C. B. *J. Phys. Chem. B* **2001**, *105*, 12068.
(31) Konecny, R.; Doren, D. J. *J. Am. Chem. Soc.* **1997**, *119*, 11098.
(32) Ellison, M. D.; Hamers, R. J. *J. Phys. Chem. B* **1999**, *103*, 6243.
(33) Barriocanal, J. A.; Doren, D. J. *J. Phys. Chem. B* **2000**, *104*, 12269.
(34) Jung, Y. S.; Choi, C. H.; Gordon, M. S. *J. Phys. Chem. B* **2001**, *105*, 4039.
(35) Lee, C. T.; Yang, W. T.; Parr, R. G. *Phys. Rev. B* **1988**, *37*, 785.
(36) Becke, A. D. *J. Chem. Phys.* **1993**, *98*, 5648.
(37) Schwartz, M. P.; Ellison, M. D.; Coulter, S. K.; Hovis, J. S.; Hamers, R. J. *J. Am. Chem. Soc.* **2000**, *122*, 8529.
(38) Coulter, S. K.; Schwartz, M. P.; Hamers, R. J. *J. Phys. Chem. B* **2001**, *105*, 3079.
(39) Kim, J. H.; Yang, G.; Weiss, A. H. *Surf. Sci.* **1998**, *396*, 388.
(40) Lampe, F. W.; Franklin, J. L.; Field, F. H. *J. Am. Chem. Soc.* **1957**, *79*, 6129.
(41) Weser, T.; Bogen, A.; Konrad, B.; Schnell, R. D.; Schug, C. A.; Steinmann, W. In *Proceedings of the 18th International Conference on the Physics of Semiconductors*; Engström, O., Ed.; World Scientific Publishing: Singapore, 1987.
(42) Weser, T.; Bogen, A.; Konrad, B.; Schnell, R. D.; Schug, C. A.; Moritz, W.; Steinmann, W. *Surf. Sci.* **1988**, *201*, 245.
(43) Papageorgopoulos, A.; Corner, A.; Kamaratos, M.; Papageorgopoulos, C. A. *Phys. Rev. B* **1997**, *55*, 4435.
(44) Miki, K.; Sakamoto, K.; Sakamoto, T. *Appl. Phys. Lett.* **1997**, *71*, 3266.
(45) Lin, D. S.; Wu, P. H. *Surf. Sci.* **1998**, *397*, L273.
(46) Norenberg, H.; Briggs, G. A. D. *Surf. Sci.* **1999**, *430*, 154.
(47) Moriarty, P.; Koenders, L.; Hughes, G. *Phys. Rev. B* **1993**, *47*, 15950.
(48) Miki, K.; Owen, J. H. G.; Bowler, D. R.; Briggs, G. A. D.; Sakamoto, K. *Surf. Sci.* **1999**, *421*, 397.
(49) Leifeld, O.; Grutzmacher, D.; Muller, B.; Kern, K.; Kaxiras, E.; Kelires, P. C. *Phys. Rev. Lett.* **1999**, *82*, 972.
(50) Simon, L.; Stoffel, M.; Sonnet, P.; Kubler, L.; Stauffer, L.; Selloni, A.; De Vita, A.; Car, R.; Pirri, C.; Garreau, G.; Aubel, D.; Bischoff, J. L. *Phys. Rev. B* **2001**, *6403*, 035306.
(51) Gutleben, H.; Lucas, S. R.; Cheng, C. C.; Choyke, W. J.; Yates, J. T. *Surf. Sci.* **1991**, *257*, 146.
(52) Cheng, C. C.; Yates, J. T. *Phys. Rev. B* **1991**, *43*, 4041.
(53) Waltenburg, H. N.; Yates, J. T. *Chem. Rev.* **1995**, *95*, 1589.
(54) Cakmak, M.; Srivastava, G. P. *Phys. Rev. B* **1999**, *60*, 5497.
(55) Although we were not able to calculate dissociation of $H_2S$ on different dimers in this work, we point out that previous experimental and theoretical work[23−26] has indicated that full dissociation of $H_2S$ onto different dimers does occur. There have been, however, no previous kinetics calculations on the full dissociation pathways of the channels involving different Si dimers. Clearly more work is needed even for this simple system.
(56) Nuzzo, R. G.; Fusco, F. A.; Allara, D. L. *J. Am. Chem. Soc.* **1987**, *109*, 2358.
(57) Jung, C.; Dannenberger, O.; Xu, Y.; Buck, M.; Grunze, M. *Langmuir* **1998**, *14*, 1103.
(58) Szafranski, C. A.; Tanner, W.; Laibinis, P. E.; Garrell, R. L. *Langmuir* **1998**, *14*, 3570.
(59) Bandyopadhyay, K.; Vijayamohanan, K.; Venkataramanan, M.; Pradeep, T. *Langmuir* **1999**, *15*, 5314.
(60) Glass, J. A.; Wovchko, E. A.; Yates, J. T. *Surf. Sci.* **1995**, *338*, 125.
(61) Xie, Z. X.; Uematsu, Y.; Lu, X.; Tanaka, K. *Phys. Rev. B* **2002**, *66*, 125306.
(62) Chadi, D. J. *Phys. Rev. Lett.* **1979**, *43*, 43.
(63) Liu, Q.; Hoffmann, R. *J. Am. Chem. Soc.* **1995**, *117*, 4082.
(64) Konecny, R.; Doren, D. J. *J. Chem. Phys.* **1997**, *106*, 2426.
(65) Widjaja, Y.; Musgrave, C. B. *Surf. Sci.* **2000**, *469*, 9.